Realistic Solar Disc Rendering

Andrei Linţu Jörg Haber Marcus Magnor

Max-Planck-Institut für Informatik
Stuhlsatzenhausweg 85
D-66123 Saarbrücken

lintu@mpi-sb.mpg.de haberj@mpi-sb.mpg.de magnor@mpi-sb.mpg.de

ABSTRACT

This paper concentrates on rendering the solar disc considering Rayleigh scattering, Mie scattering, absorption, and refraction. The atmosphere is modeled in layers, each layer having a set of individual optical properties. Based on different atmospheric temperature profiles and climates, the solar disc is rendered in realistic shape and color. In particular, we replicate optical phenomena such as the red and the green flash, limb darkening, and refractive distortions of the solar disc.

Keywords

Photo-realistic rendering, scattering, solar disc, atmosphere, ray-tracing

1. INTRODUCTION

Computing a physically and visually correct reproduction of the colors of the sky dome around the observer is an essential task for outdoor scene renderings. Although some work has been done on the simulation of the sky colors during daytime [PSS99; NDKY96], nighttime [WJDS+01], and twilight periods [HMS04], realistic rendering of the solar disc has received little attention in the literature so far. In order to achieve realistic renderings, the optical phenomena occurring in the atmosphere need to be considered. Based on the physical structure of the Earth's atmosphere, this paper reproduces solar disc appearances at sunrise/sunset in correct form and color.

Permission to make digital or hard copies of all or part of his work for personal or classroom use is granted without fee provided that copies are not made or distributed for profit or commercial advantage and that copies bear this notice and the full citation on the first page. To copy otherwise, or republish, to post on servers or to redistribute to lists, requires prior specific permission and/or a fee.

Conference proceedings ISBN 80-903100-7-9

WSCG'2005, January 31-February 4, 2005

Plzen, Czech Republic.

Copyright UNION Agency - Science Press

Figure 1: A sunset scenario in a polluted maritime climate, few minutes before the Sun is setting.

We take into account Rayleigh scattering due to air molecules as well as Mie scattering due to aerosols present in the atmosphere, thus obtaining a realistic color of the solar disc. To obtain the correct shape of the solar disc, we also model refraction, allowing us to trace rays correctly through the atmosphere.

Based on the actual structure of a given input atmosphere model, i.e. height-dependent temperature profile and distribution of aerosols, we ob-

serve different colors and shapes of the solar disc. The color of the disc varies with the climate, its shape differs due to mirage phenomena. By rendering the Sun taking different wavelengths into account, chromatic abberation phenomena such as the green flash or the red flash can be reproduced.

In the following Section we give a short overview of previous work in the field of physically based rendering methods of the solar disc and the atmosphere. After an introductory review of the physics in Section 3, we give a system overview in Section 4. We describe our approach on solar disc rendering in Section 5. Results are presented in Section 6, before we conclude and point to future work in Section 7.

2. RELATED WORK

Realistic renderings of atmospheric phenomena has been a well researched topic in the computer graphics community. We review papers focusing on solar disc rendering, as well as work on rendering the sky.

Some publications focus on physically correct and realistic atmosphere simulations, for daytime [PSS99], [NDKY96] as well as for nighttime [WJDS+01]. Also, a system for rendering the atmosphere from a viewpoint situated in space is presented by Nishita *et al.* [NSTN93].

These approaches concentrate on fast rendering of the atmosphere, approximating the physics of atmospheric light transport. A work focusing on a physically correct simulation of the atmosphere during twilight phenomena is presented in [HMS04].

A different method focusing on the rendering of the solar disc is presented by Bruton [Bru96]. In his thesis, ray-tracing through the atmosphere is performed using Lehn's model [Leh85], and solar disc appearance is simulated from diverse input temperature profiles. However, this work considers only Rayleigh scattering due to air molecules. Thus, different types of sunsets depending on current aerosol distribution in the atmosphere cannot be simulated.

One possible approach is to simulate the green flash using an approach based on photon mapping [GSAM04], this work implements a "Curved Photon Mapping" algorithm. Although the obtained result is highly realistic, this approach is slow (due to the photon mapping algorithm), and it lacks any dependence on climate conditions.

In contrast, our approach concentrates on combining the simplified parabolic model for ray-tracing in the atmosphere presented by Lehn [Leh85] and the climate dependent stratified atmosphere model presented in [HMS04] in order to create a ray-tracing system which realistically reproduces several possible sequences of the solar disc at sunset or sunrise.

3. SUNSET SCIENCE

Our approach for rendering the solar disc is able to faithfully reproduce a variety of optical phenomena such as mirages and chromatic abberations. In the following, we give physical descriptions of these phenomena.

3.1 Mirages

Mirages are caused by strong ray-bending due to steep temperature gradients in the atmosphere. According to the position of the mirrored images relative to the original object, mirages can be classified into two main categories:

- inferior mirages: mirrored image below object
- superior mirages: mirrored image above object

The *inferior mirage* occurs if a layer of hot air is close to the ground, bending the grazing rays upwards. It can be observed in deserts or above asphalt pavings on sunny days. An example of this mirage is presented in Figure 4, the so called *Omega sunset*.

For the *superior mirage* to take place, the observer has to be situated *inside* a layer of air with a thermal inversion, i.e. there is a sudden increase in temperature above the observer. The rays in this duct intersect after traversing kilometers through the atmosphere, creating the inverted image of a distant object. In the case of the superior mirage, the intersecting rays remain inside the inversion layer. Thus superior mirages do not occur of astronomical objects that are situated outside the Earth's atmosphere.

If the observer is above a thermal inversion layer the just recently understood *mock mirage* can occur [You04]. In this case the intersecting rays can escape the Earth's atmosphere, the intersection points being far away from the observer.

A large variety of mirages can occur. They are highly dependent on the altitude of the observer. In order to be able to see a solar disc mirage, at least one temperature inversion layer has to be present in the atmosphere at the time of observation. This inversion layer produces a sudden change in the refraction index of the air, thus creating a mirage.

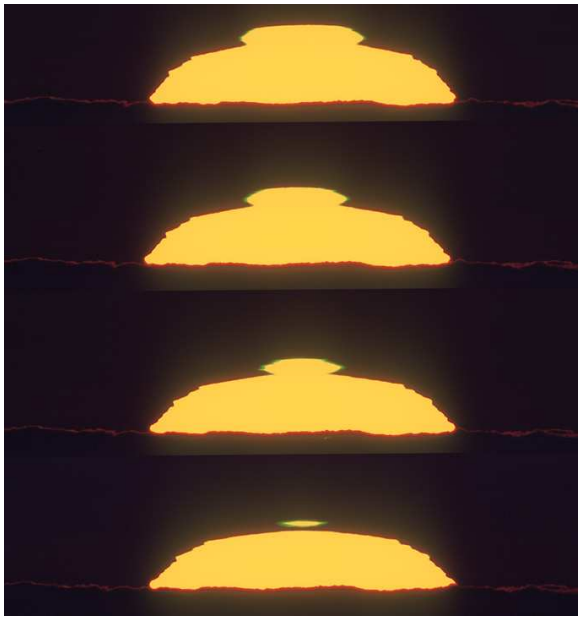

Figure 2: Photograph of a Green Flash Sequence
Photograph by Mario Cogo, `www.intersoft.it/galaxlux`, used with permission

3.2 The Green Flash

This peculiar optical phenomenon consists of a short green flash (lasting only a few seconds) that can appear on top of the solar disc when the Sun sets. It is due to the large variation of refraction and induced dispersion close to the horizon.

There are several types of green flashes, each one being associated with a mirage phenomenon. The green color is mainly due to *atmospheric dispersion* which makes the red component of the light spectra disappear first, followed by green, blue, and violet during sunset. Another effect contributing to the green flash is *atmospheric extinction*, which mainly consists of *atmospheric scattering* due to air molecules. In this case, the shortest wavelengths are almost completely removed. Therefore, it is sometimes possible to observe only the *green* component of the light spectra for a few seconds during sunset.

The green flash phenomenon depends also on the adaptation of the human visual system during observation. The high intensity of the solar disc bleaches the red-sensitive photo-pigments on the retina, thus allowing also yellow flashes to be perceived as green.

In Figure 2 a sequence of photographs of this phenomenon are presented. Figure 13 illustrates a simulation generated using our system. An exhaustive explanation and bibliography of this phenomenon can be found in [You04].

Figure 3: Photograph of a Red Flash
Photograph by Mario Cogo, `www.intersoft.it/galaxlux`, used with permission

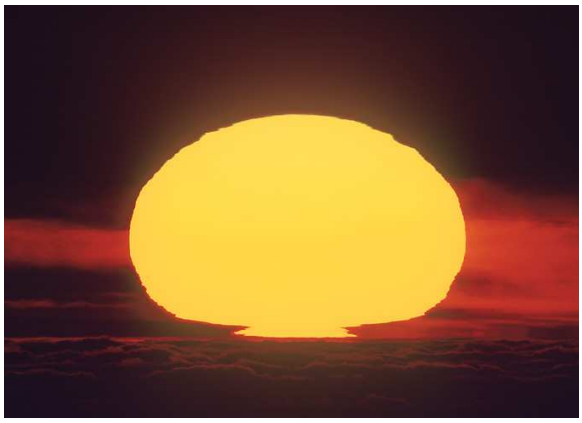

Figure 4: Photograph of an Omega Sun
Photograph by Mario Cogo, `www.intersoft.it/galaxlux`, used with permission

3.3 The Red Flash

Another type of mirage, which is harder to observe than the green flash, is the red flash. The red flash can occur due to a *mock mirage*, where it consists of a round red "droplet" below the "cropped" solar disc (see Figure 3), or as a consequence of an *inferior mirage*, where it is visible as a red middle region of the *Omega sunset* (see Figure 11).

3.4 Limb Darkening

This phenomenon consists of the darkened outer rim of the solar disc. It is due to the fact that light from the center of the Sun traverses less gas of the Sun's photosphere where it is partially absorbed.

Limb darkening can be phenomenologically described by

$$I'(\lambda) \;=\; I(\lambda) \cdot \left(1 - u \cdot \left(1 - \sqrt{1 - \frac{d^2}{r^2}}\right)\right) ,$$

where I is the solar irradiance, d is the distance from the center of the Sun, r is the radius of the solar disc, and u is the limb darkening coefficient for the Sun, which is approximately 0.6 for visible sunlight [Bru96].

We incorporate limb darkening in our system in order to obtain realistic renderings of the solar disc.

4. SYSTEM OVERVIEW

Our solar disc rendering system combines tracing of parabolic rays through the atmosphere [Leh85; Bru96] with an atmosphere model incorporating different climate-dependent characteristics [HMS04] to reproduce both the correct *shape* of the solar disc and its corresponding correct *color*. The used atmosphere model incorporates the scattering and absorption coefficients for Rayleigh scattering and Mie scattering. The effects of different climate types, air humidities, and atmosphere temperature profiles on the appearance of the solar disc at sunset or sunrise are simulated.

Ray-tracing through the atmosphere is computed using Lehn's parabolic model for a light ray traveling through an atmosphere layer [Leh85]. This model reduces the amount of computation time otherwise required to solve the Eikonal PDE for light rays traveling through the atmosphere. To determine the distribution of the aerosols in the atmosphere we use the OPAC software package [HKS98; Hes98].

As input to our simulations, in addition to the required climate type and temperature profile, we also specify *observer height*.

We now give a short, step by step description of the used method:

- specify input: *temperature profile*, *climate*, *number of layers* and *observer height*;
- precompute the *radius of curvature* for the parabolic ray approximations;
- compute *solar disc shape* – ray-trace through the atmosphere model and compute the length the rays travel through each layer;
- compute *solar disc color* – multiply the initial intensity with the extinction factor;

5. SOLAR DISC RENDERING

In this section we describe the atmosphere model and the ray-tracing mechanism used in our simulations.

5.1 Extinction Coefficients

To determine the optical properties of the *aerosols* present in the atmosphere, we use the publicly available OPAC software package [HKS98; Hes98]. Using this package we compute wavelength-dependent aerosol absorption coefficients $\sigma_a^{\text{aerosol}}(\lambda)$, scattering coefficients $\sigma_s^{\text{aerosol}}(\lambda)$, and anisotropy factors $g(\lambda)$ for the given input climate type of an arbitrary aerosol composition and humidity.

Values for the wavelength-dependent scattering coefficient $\sigma_s^{\text{air}}(\lambda)$ of *air* molecules are taken from Nagel *et al.* [NQKW78]. Pure air does not significantly absorb visible light. Thus, the extinction coefficient of air σ_e^{air} is assumed to be equal to the scattering coefficient, $\sigma_e^{\text{air}}(\lambda) = \sigma_s^{\text{air}}(\lambda)$.

5.2 Atmosphere Model

The atmosphere model used in our system is stratified, consisting of atmosphere layers located geocentrically around the surface of the Earth.

The height of individual layers is chosen such that approximately the same amount of molecules is contained in each one of them. Our atmosphere model reaches up to a height of $H_{\max} = 35\,\text{km}$. The number of molecules above this height can be considered negligible. A schematic description of the used model is depicted in Figure 5.

We discretize the atmosphere into a set of geocentric atmosphere layers $L_i, (i = 1, \ldots, N)$. Each layer L_i has an individual upper and lower boundary at height $H_{i,\max}$ and $H_{i,\min}$, respectively. To each layer L_i we assign the relative humidity w_i and the following optical parameters:

- aerosol scattering coefficient $\sigma_{s,i}^{\text{aerosol}}(\lambda)$ and extinction coefficient $\sigma_{e,i}^{\text{aerosol}}(\lambda) = \sigma_{s,i}^{\text{aerosol}}(\lambda) + \sigma_{a,i}^{\text{aerosol}}(\lambda)$;
- Henyey-Greenstein scattering anisotropy coefficient $g_i(\lambda)$;
- isotropic scattering coefficient of air $\sigma_{s,i}^{\text{air}}(\lambda)$;
- mean index of refraction $\eta_i(\lambda)$ and indices of refraction $\eta_{i,\min}(\lambda)$ and $\eta_{i,\max}(\lambda)$ corresponding to $H_{i,\min}$ and $H_{i,\max}$, respectively.

All these parameters are functions of the wavelength λ and are evaluated for a discrete number of wavelengths. A more detailed description of the used layered atmosphere model can be found in [HMS04].

The simulations presented in this paper are typically computed using 300–30000 layers, depending on the input temperature profile. The number of input layers is dependent on the height of

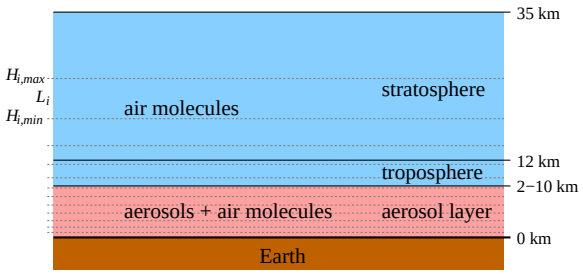

Figure 5: Cross section of the atmosphere model. It is composed of an aerosol-containing region, clear troposphere and stratosphere [HKS98]. For the aerosol region the height is climate dependent.

the inversion layers. For a thermal inversion layer close to the surface of the Earth, we need a fine sampling of our atmosphere model in order to be able to correctly simulate the corresponding mirage, due to the exponential distribution of the atmosphere layers.

The solar irradiance $I_0(\lambda)$ outside the atmosphere, i.e. before the sun light reaches the ozone layer, is computed from the solar spectrum data measured by Kurucz [KFBT84] for wavelengths from 200 nm to 1000 nm. We filter the solar irradiance using the approach presented in [HMS04], accounting for wavelength-dependent absorption in the ozone layer.

5.3 Temperature Profiles

Our simulations are based on temperature profiles of the atmosphere, the starting point being the U.S. Standard Atmosphere [Bru96; You04]. In order to simulate different mirage phenomena, several input height-temperature profiles differing from the U.S. Standard Atmosphere are used. The profile of the atmosphere is specified as the temperature gradient at discretized heights.

5.4 Atmospheric Refraction

A model based on exact computation of refraction taking place in the atmosphere requires numerically solving a PDE and is computationally too expensive to be practically useful. The simplest solution is to assume all rays traveling linearly through each layer. We chose to implement a quadratic-error model developed by Lehn [Leh85]. This model assumes that the circular arcs representing the Earth's surface, the light rays, and the layer boundaries of the atmosphere model can be locally approximated by parabolas.

For each layer L_i we precompute the wavelength-dependent radius of curvature $\kappa_i(\lambda)$ using

$$\kappa_i(\lambda) \;=\; -K \cdot \eta_i(\lambda) \cdot \frac{(H_{i,\max} - H_{i,\min})}{(\eta_{i,\max}(\lambda) - \eta_{i,\min}(\lambda))} \;,$$

where $\eta_i(\lambda)$ is the mean index of refraction of air in layer L_i, and $\eta_{i,\max}(\lambda)$, $\eta_{i,\min}(\lambda)$ are the refractive indices of air corresponding to the upper and lower heights $H_{i,\max}$ and $H_{i,\min}$. The value for K depends on the initial parameters in the ray-tracing process and can be found in Bruton's thesis [Bru96]. The rays are traced through the atmosphere starting from the layer containing the observer.

In Figure 6, the two possible cases of the intersection between the currently traced ray and the boundaries of an atmosphere layer are depicted. The expected trajectory of the ray is denoted as Path 1. However, if a thermal inversion is present, the ray can bend downwards following Path 2.

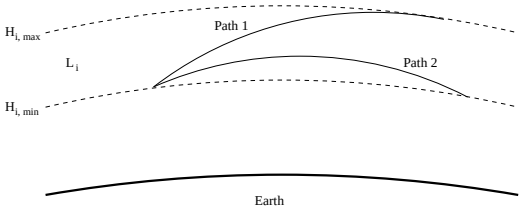

Figure 6: Two possible ray paths through the atmosphere. Path 1 depicts the normal trajectory of a ray traveling through layer L_i. For a thermal inversion present in L_i, the ray trajectory may follow the path indicated as Path 2.

The distance $\Delta\gamma_i(\lambda)$ that a light ray of wavelength λ travels through layer L_i is numerically determined by

$$\Delta\gamma_i(\lambda) \;=\; 2 \cdot \kappa_i(\lambda) \cdot \arcsin\left(\frac{d}{2 \cdot \kappa_i(\lambda)}\right) \qquad (1)$$

with

$$d \;=\; \sqrt{\Delta x^2 + \left(\Delta z - \frac{\Delta x^2}{2R}\right)^2} \;.$$

The values for Δx and Δz are computed during the ray-tracing process through the atmosphere layers as described by Lehn [Leh85] and Bruton [Bru96]. Based on the current optical parameters during ray-tracing, for each layer L_i a decision is taken [Leh85; Bru96] whether Path 1 or Path 2 is chosen for the current ray (see Figure 6).

In order to accurately compute the indices of refraction for each atmosphere layer based on the input temperature profiles, we employ the formulas proposed by Ciddor [Cid96]:

$$\eta_{h,w}(\lambda) \;=\; 1 \;+\; \frac{\rho_{\mathrm{a}}}{\rho_{\mathrm{d}}} \cdot (\tilde{\eta}_{\mathrm{d}} - 1) \;+\; \frac{\rho_{\mathrm{v}}}{\rho_{\mathrm{w}}} \cdot (\tilde{\eta}_{\mathrm{w}} - 1) \;,$$

where ρ_{d} is the density of dry air at 15 °C and 101325 Pa, ρ_{w} is the density of pure water vapor at 20 °C and 1333 Pa, and ρ_a and ρ_v are the densities of the dry air component and water vapor component for the current conditions. The equations needed to calculate the air densities in the above formula are given by Ciddor [Cid96]. To compute the values for $\tilde{\eta}_{\mathrm{d}}$ and $\tilde{\eta}_{\mathrm{w}}$, the following equations are used [Cid96]:

$$\tilde{\eta}_{\mathrm{d}}(\lambda) = 1 + \left(\frac{5792105.0}{238.0185 - \lambda^{-2}} + \frac{167917.0}{57.362 - \lambda^{-2}} \right) \cdot 10^{-8}$$

$$\tilde{\eta}_{\mathrm{w}}(\lambda) = 1 + (295.235 + 2.6422\,\lambda^{-2} - 0.03238\lambda^{-4} + 0.004028\,\lambda^{-6}) \cdot 1.022 \cdot 10^{-8} .$$

5.5 Atmospheric Extinction

To accurately determine the color of each pixel in the rendered images, we first compute the intensity $I(\lambda)$ of sun rays that reach the observer *after extinction* in the atmosphere according to:

$$I(\lambda) = I_0(\lambda) \cdot \xi_\gamma(\lambda) , \qquad (2)$$

where $I_0(\lambda)$ is the solar irradiance filtered by absorption in the ozone layer and the extinction factor $\xi_\gamma(\lambda)$ is given as:

$$\xi_\gamma(\lambda) = \exp\left(- \int_\gamma \left(\sigma_e^{\mathrm{aerosol}}(\lambda) + \sigma_e^{\mathrm{air}}(\lambda) \right) \mathrm{d}s \right) .$$

The value for the extinction factor $\xi_\gamma(\lambda)$ is numerically determined by

$$\xi_\gamma(\lambda) = \exp\left(- \sum_{i=1}^{N} \left(\sigma_{e,i}^{\mathrm{aerosol}}(\lambda) + \sigma_{e,i}^{\mathrm{air}}(\lambda) \right) \cdot \Delta\gamma_i(\lambda) \right) , \qquad (3)$$

where $\Delta\gamma_i(\lambda)$ denotes the path length through layer L_i, see Equation (1).

We take into account both multiple Rayleigh scattering (by air molecules) and Mie scattering (by aerosols). Mie scattering is modeled using the well-known Henyey-Greenstein approximation [HG41]. For rendering the solar disc, the phase angle (i.e. the angle between incident light and scattering direction) in this approximation can be considered equal to zero, since the diameter of the solar disc is merely 0.5°. As a consequence, the extinction factor $\xi_\gamma(\lambda)$ from Equation (3) is modified as follows:

$$\xi'_\gamma(\lambda) = \exp\left(- \sum_{i=1}^{N} \sigma_{e,i}^{\mathrm{mult}}(\lambda) \cdot \Delta\gamma_i(\lambda) \right) , \qquad (3')$$

$$\sigma_{e,i}^{\mathrm{mult}}(\lambda) = (1 - g(\lambda)) \cdot \sigma_{e,i}^{\mathrm{aerosol}}(\lambda) + \sigma_{e,i}^{\mathrm{air}}(\lambda) .$$

Substituting $\xi'_\gamma(\lambda)$ for $\xi_\gamma(\lambda)$ in Equation (2) yields the final formula to compute the intensity $I(\lambda)$.

5.6 Gamma Correction

For the final rendering, we convert the sampled spectral distribution into its corresponding color in XYZ color space by convolution with the CIE (1964) 10° color matching functions. Due to the high dynamic range of intensities, we have to apply gamma correction to faithfully display our results. We thus transform from XYZ color space to xyY color space and perform gamma-correction on the Y-value:

$$\mathrm{Y}' = \mathrm{Y}^{1/\gamma} ,$$

where we use $\gamma = 2.5$ for the correction coefficient. Finally, we convert back to XYZ and from XYZ to RGB color space using the sRGB primaries from CIE Rec. 709 and a D_{65} whitepoint. For details of these spectral conversions see the textbooks by Wyszecki *et al.* [WS82] or Hall [Hal89].

6. RESULTS

We have rendered a variety of sunset sequences for different meteorological conditions using the approach presented in this paper. To obtain a large diversity of solar disc renderings, various aerosol distributions, air humidity values, and temperature profiles of the atmosphere have been used.

Figure 1 shows a sunset scenario for a polluted maritime climate with 80% humidity. A polluted urban climate with 80% humidity has been used to simulate the sunset depicted in Figure 7. The sunset reproduced in Figure 8 has been simulated for a continental climate with 70% humidity. For all of the above mentioned images, the colors of the sky have been computed and rendered using the approach presented in [HMS04].

All images presented in this paper have been generated using a discretization of $N_\lambda = 8$ wavelengths in the range from 380 nm to 720 nm. Depending on the number N of atmosphere layers used for the simulations and the resolution of the generated images, computation times on a 2.4 GHz Pentium4 PC are in the range of a few minutes for our unoptimized implementation.

Figures 9 and 10 show the effect of varying humidity on the appearance of the solar disc at sunset or sunrise. With increasing air humidity the solar disc becomes noticeably darker.

The consequences of a temperature inversion layer close to the ground is depicted in Figure 11.

Figure 7: Sunset in a polluted urban climate with 80% humidity.

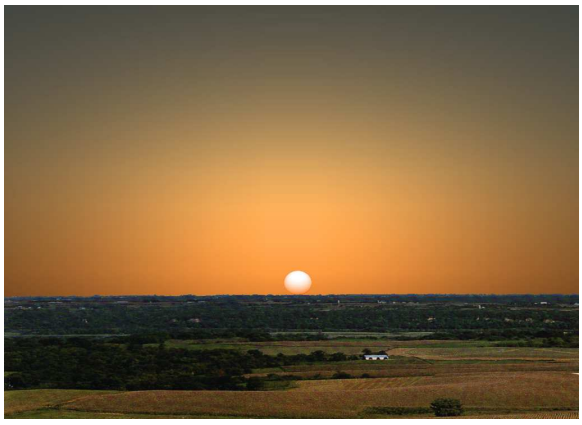

Figure 8: Sunset for a continental climate with 70% humidity.

This is the so called *Omega Sun*, the form of the solar disc being reminiscent of the Greek letter Ω.

The red flash is simulated in Figure 12. An atmosphere containing a weak inversion layer is used here to simulate a mock mirage for an observer situated at an altitude of 45 m above sea level.

In Figure 13, a green flash is replicated. The atmosphere is identical to the one used in Figure 12. Here, however, the Sun is at a lower altitude. The difference in altitude between successive renderings is below one arc-minute.

7. CONCLUSIONS

A system for realistic rendering of the solar disc has been presented. Atmospheric optical phenomena such as mirages, red and green flash, and limb darkening are simulated based on physical laws and meteorological conditions. In order to validate the obtained results, one future research direction is to calibrate the rendered images with real life photographs of sunsets. Furthermore, due to the large variation in extinction of various climates, which are reflected in the high dynamic range of our obtained results, an efficient tone mapping operator should be developed.

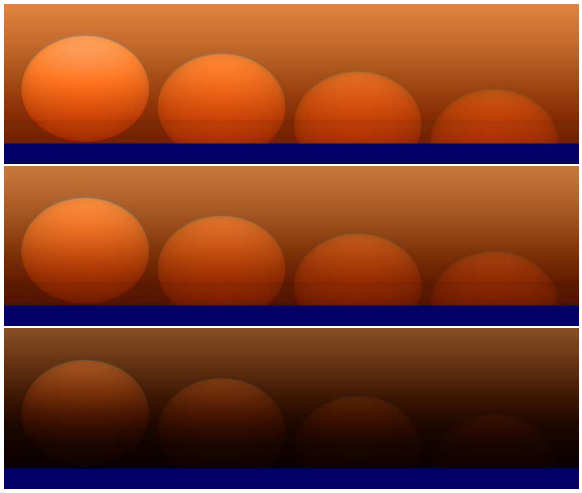

Figure 9: Sunset in continental climate for different humidities. Top to bottom: 50%, 80%, and 95% humidity.

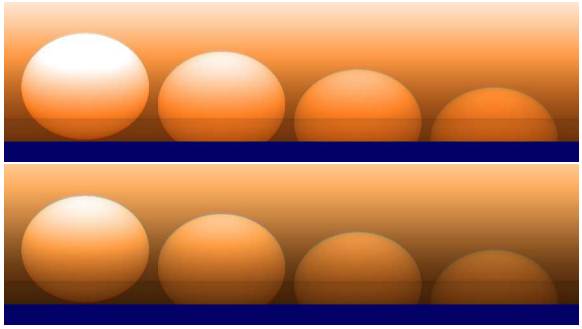

Figure 10: Sunset in tropical maritime climate for 80% (top) and 90% (bottom) humidity.

Acknoledgements

The authors would like to thank Mario Cogo for his kind permission to use his photographs of the sun [Cog04].We also thank Andrew T. Young for sharing his comprehensive knoledge about the Green Flash of his page [You04].

8. REFERENCES

[Bru96] Dan Bruton. *Optical Determination of Atmospheric Temperature Profiles*. PhD thesis, Texas A&M University, August 1996.

[Cid96] Philip E. Ciddor. Refractive index of air: new equations for the visible and near infrared. *Applied Optics*, 35(9):1566–1573, March 1996.

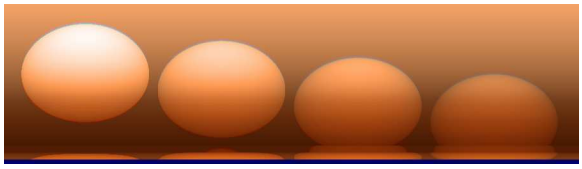

Figure 11: The omega sun frequently occurs in desert climates. A strong inversion layer right above the ground causes this inferior mirage.

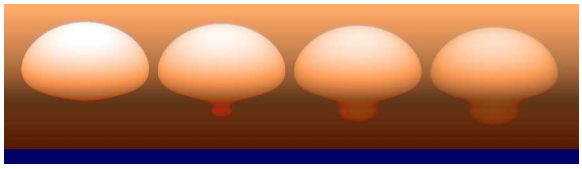

Figure 12: The red flash—a frequent mirage, hardly observed because of the small hue difference between the color of the solar disc and that of the flash.

[Cog04] Mario Cogo. Astrophotography. available from `http://www.intersoft.it/galaxlux`, 1996 - 2004.

[GSAM04] D. Gutierrez, F. Seron, O. Anson, and A. Munoz. Chasing the Green Flash: a Global Illumination Solution for Inhomogeneous Media. In *Spring Conference On Computer Graphics 2004*, pages 95–103, 2004.

[Hal89] Roy Hall. *Illumination and Color in Computer Generated Imagery*. Springer, New York, 1989.

[Hes98] M. Hess. OPAC (Optical Properties of Aerosols and Clouds). available from `ftp://ftp.lrz-muenchen.de/pub/science/meteorology/aerosol/opac/`, 1998.

[HG41] Louis G. Henyey and Jesse L. Greenstein. Diffuse Radiation in the Galaxy. *Astrophysical Journal*, 93:70–83, 1941.

[HKS98] M. Hess, P. Koepke, and I. Schult. Optical Properties of Aerosols and Clouds: The Software Package OPAC. *Bulletin of the American Meteorological Society*, 79(5):831–844, May 1998.

[HMS04] Jörg Haber, Marcus Magnor, and Hans-Peter Seidel. From Dust to Dawn — Physically based Simulation of Twilight Phenomena. *Conditionally Accepted to ACM Transactions on Graphics*, 2004.

[KFBT84] R. L. Kurucz, I. Furenlid, J. Brault, and L. Testerman. Solar Flux Atlas from 296 to 1300 nm. Technical report, NOAO, Sunspot, NM, 1984. available from `http://kurucz.harvard.edu/sun/fluxatlas/`.

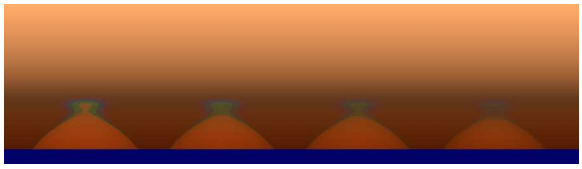

Figure 13: The green flash resulting from a mock mirage.

[Leh85] W. H. Lehn. A simple parabolic model for optics of the atmospheric surface layer. *Applied Mathematical Modelling*, 9:447–453, December 1985.

[NDKY96] Tomoyuki Nishita, Yoshinori Dobashi, Kazufumi Kaneda, and Hideo Yamashita. Display Method of the Sky Color Taking into Account Multiple Scattering. In *Proc. Pacific Graphics '96*, pages 117–132. IEEE, 1996.

[NQKW78] M. R. Nagel, H. Quenzel, W. Kwet, and R. Wendling. *Daylight Illumination — Color-Contrast Tables for Full-Form Objects*. Academic Press, New York, 1978.

[NSTN93] Tomoyuki Nishita, Takao Sirai, Katsumi Tadamura, and Eihachiro Nakamae. Display of The Earth Taking into account Atmospheric Scattering. In James T. Kajiya, editor, *Computer Graphics (SIGGRAPH '93 Conf. Proc.)*, pages 175–182. ACM SIGGRAPH, August 1993.

[PSS99] Arcot J. Preetham, Peter Shirley, and Brian Smits. A Practical Analytic Model for Daylight. In *Computer Graphics (SIGGRAPH '99 Conf. Proc.)*, pages 91–100. ACM SIGGRAPH, August 1999.

[WJDS+01] Henrik Wann Jensen, Frédo Durand, Michael M. Stark, Simon Premoze, Julie Dorsey, and Peter Shirley. A Physically-Based Night Sky Model. In *Computer Graphics (SIGGRAPH 2001 Conf. Proc.)*, pages 399–408. ACM SIGGRAPH, August 2001.

[WS82] Günter. Wyszecki and Walter S. Stiles. *Color Science: Concepts and Methods, Quantitative Data and Formulae*. John Wiley & Sons, New York, 2nd edition, 1982.

[You04] Andrew T. Young. A Green Flash Page. available from `http://mintaka.sdsu.edu/GF/index.html`, 1999 - 2004.